GRACE Follow-On accelerometer data recovery

Saniya Behzadpour[1], **Torsten Mayer-Gürr**[1], **Sandro Krauss**[1]

[1]Institute of Geodesy, Graz University of Technology

Key Points:

- Alternative processing is proposed for recovering GRACE-D accelerometer data.
- The recovered products improve overall accuracy of gravity field solutions.
- The recovered products improve the estimates of low degree zonal coefficients.

Corresponding author: Saniya Behzadpour, `behzadpour@tugraz.at`

Abstract

In Gravity Recovery and Climate Experiment (GRACE) Follow-on (GRACE-FO) mission, similar to its predecessor GRACE, the twin satellites are equipped with three-axis accelerometers, measuring the non-gravitational forces. After one month in orbit, during the in-orbit-checkout phase, the noise on GRACE-D accelerometer measurements elevated, and results in systematical degradation of the data. For this reason, the GRACE-D data needs to be replaced by synthetic data, the so-called transplant data, officially generated by the GRACE-FO Science Data System (SDS).

The SDS transplant data is derived from the GRACE-C accelerometer measurements, by applying time and attitude corrections. Furthermore, model-based residual accelerations due to thruster firings on GRACE-D were added, proven to improve the data quality in gravity field recovery. However, preliminary studies of GRACE-FO data during the single accelerometer months show that the low degree zonal harmonics, in particular C_{20} and C_{30}, are sensitive to the current transplant approach.

In this work, we present a novel approach to recover the GRACE-D ACT1B data by incorporating non-gravitational force models and analyze its impact on monthly gravity field solutions. The results show the improved ACT1B data not only contributed to a noise reduction, but also improve the estimates of the C_{20} and C_{30} coefficients. The application of this new approach demonstrates that the offset between Satellite Laser Ranging (SLR) and GRACE-FO derived C_{30} time series can be reduced by the use of the alternative accelerometer product.

1 Introduction

The Gravity Recovery and Climate Experiment Follow-On (GRACE-FO) mission (Landerer et al., 2020) was successfully started on May 22, 2018, and since then, provides high-quality observations to continue the gravity field time series of its predecessor, the GRACE mission (2002-2017) (Tapley et al., 2004). Similar to GRACE, both satellites in GRACE-FO mission are equipped with high precision accelerometers to measure the non-gravitational forces (e.g. atmospheric drag and radiation pressure), as well as disturbances due to satellite's operation, such as attitude thruster activation. With the aim of gravity field recovery, these measurements are essential to reduce the effects of non-gravitational perturbations from the orbit and obtain the sough-after gravitational components.

Early studies have shown that the accelerometer measurements (ACC) from both GRACE-FO satellites are contaminated by different types of noise. Therefore, the standard GRACE Level-1A to Level-1B processing (Wu et al., 2006) does not deliver ACC Level-1B (ACC1B) products with sufficient accuracy for gravity field recovery. For this reason, the GRACE-FO Science Data System (SDS) team has developed specific calibration process for the accelerometer on each satellite and has provided the calibrated GRACE-FO accelerometer data (ACT) products (McCullough et al., 2019). The SDS members consist of the Center for Space Research at the University Texas at Austin (CSR), NASA's Jet Propulsion Laboratory (JPL), and the German Research Centre Geosciences (GFZ).

In case of GRACE-C, the accelerometer data is calibrated throughout the mission by replacing un-realistic accelerations due to thruster firing with model-based responses and removing large geographical/orbital related accelerations, called Phantom accelerations. The same calibration process is applied to the GRACE-D data for the early days of the mission (until 2018-06-21).

However, After one month in orbit, the GRACE-D accelerometer data degraded. Hence, its measurements were replaced by synthetic data, the so-called transplant data.

The transplant approach, initially studied and developed for GRACE, uses one satellite's ACC measurement to generate the other twin satellite ACC data. The idea originates from the GRACE mission in 2002 and 2003, when over two periods of several weeks, only one accelerometer data was available. Save et al. (2006) showed that the transplant procedure is feasible because both satellites fly in the same orbit and have a time delay of 25-30 s. Therefore, the change in the non-gravitational accelerations during this time delay is very small, and both accelerometers would measure approximately the same signal. However, it is mandatory to apply time and attitude corrections to the available accelerometer measurements, to account for the variable separation between the two spacecrafts and the orientation differences relative to each other.

Over the final months of GRACE, after the GRACE-B accelerometer was turned off due to battery issues, the demand for synthetic ACC data raised once again. Bandikova et al. (2019) presented an improved ACC data transplant approach, which includes the modeling of residual linear accelerations due to thruster firings, in addition to the attitude and time correction. The modeling of thruster spikes has been studied before both on ACC1B (Meyer et al., 2011) and ACC Level-1A (ACC1A) (McCullough et al., 2015) using a statistical approach. However, Bandikova et al. (2019) show that by determining the dynamic system, which generates the impulse response of each thruster pair, one can improve the estimates of the spikes and reduce the noise in gravity field solutions. The improved ACC transplant contributes to the processing standards for final months of GRACE, and ACC transplant data was included in the official Level-1B products.

Based on the official Level-1B products, GRACE/GRACE-FO Level-2 RL06 products, are provided by the SDS members. To provide long-term gravity field time series, the processing standards for GRACE-FO remained mostly consistent with GRACE. In addition to the official centers, various other research institutions are also preparing their processing setup for GRACE-FO gravity field solutions. Among these centers, the Institute of Geodesy at Graz University of Technology (TUG) routinely provides operational GRACE-FO products, consistent with ITSG-Grace2018 standards (Kvas, Behzadpour, et al., 2019), which are published by the International Centre for Global Earth Models (ICGEM, (Drewes et al., 2016)).

Preliminary analysis of GRACE-FO data during the single accelerometer months proves that the derived low degree zonal harmonics, in particular C_{20} and C_{30}, are affected by the transplant approach, and as recommended by SDS, are needed to be replaced by SLR-derived values (Loomis et al., 2020). Figure 1 shows the absolute difference between GRACE-FO derived C_{30} and SLR-derived time-series, provided in the Technical Note-14 (TN-14), and compares their variations with β' angle of the orbit. The β' angle represents the angle between the orbital plane of the satellite and the Sun direction. It is visible that the peaks, indicating the largest deviations from the recommended values, are highly correlated with the periods with β' angle close to zero. During these periods, the satellite is exposed to direct sunlight for approximately half of its revolution, and the rest of the time is passing through the Earth's shadow, causing large temperature differences. This orbital condition with 161-day cycle has an effect on satellite's operation, specifically on the energy absorption by solar panels and on the thermal control due to the heating by the Sun.

To further investigate the reason, the transplant approach can be evaluated in GRACE mid-timespan, when both accelerometers operated nominally and provided high-quality data. Meyer et al. (2011) compared the acceleration signal measured by each satellite in the same orbit position during a half-cycle of β' angle between March and September 2007. They showed that a difference up to 3 nm/s^2 exists between the two measured signals. The most substantial difference happens for a short period of time when satellites are transiting through Earth's shadow, as the solar radiation pressure (SRP) changes for each satellite at the same position. Additionally, a long-term variation exists mainly during periods when β' angle is close to zero. In other words, when satellites are under direct Sun exposure, due to high fluctuations in the atmosphere density, they

Figure 1. Absolute difference between GRACE-FO estimated C_{30} and recommended values in TN-14. The largest deviations are correlated with β' angle close to zero.

experience different forces, which in this case, is the drag force. Hence, the direct transplanting of ACC data can cause large errors under these conditions.

The main purpose of this paper is to present an improved method to recover the GRACE-D accelerometer data by incorporating non-gravitational force models and analyze its impact on the recovered gravity field solutions. Within the gravity field recovery, the transplanted GRACE-D accelerometer data shows a significant impact on the low degree coefficients, in particular reduces the offset between SLR and GRACE-FO derived C_{30} time series.

The paper is organized as follows: In Section 2, we provide a brief overview about the accelerometer data and focus on different ACC data products. In Section 3, we briefly describe the non-gravitational forces acting on the satellites. In Section 4, we present the alternative GRACE-D ACC recovery. And finally, in Section 5, we discuss the results by comparing our products with the official transplant data and their impact on the recovered gravity field solutions.

2 Accelerometer data

The GRACE-FO accelerometer is a three-axis electrostatic accelerometer manufactured by the Office National d'Études et de Recherches Aérospatiales (ONERA) (Christophe et al., 2015). The accelerometer provides information about the linear and angular acceleration of the satellite. The sensor has two high-sensitive axes, the radial and along-track axes exhibiting a resolution better than 0.1 $\mathrm{nm}/(\mathrm{s}^2\sqrt{\mathrm{Hz}})$, and one less-sensitive axis, the cross-track axis with an accuracy of 1 $\mathrm{nm}/(\mathrm{s}^2\sqrt{\mathrm{Hz}})$.

The accelerometer is placed in the center of mass (CoM) of the satellite. The core of the sensor consists of a proof mass, surrounded by an electrode cage. The proof mass is suspended by electrostatic forces generated by the electrodes. The sensor measurement is determined from the usage of analog voltages, producing the electrostatic force. The electrostatic force is proportional to the sum of the non-gravitational forces acting on the satellite, including atmospheric drag, solar radiation pressure (SRP), earth radiation pressure (ERP), and other disturbances.

There are three types of science data products for the GRACE-FO accelerometer data, which in the following, will be briefly introduced.

2.1 ACC1A

The ACC Level-1A (ACC1A) data products include the 10-Hz linear acceleration measurements, given in accelerometer reference frame (AF). The origin of this frame is defined to be the center of mass of the proof mass and the frame axes are directed as shown by Figure 2. The time frame of the data is determined by the on-board computer (OBC).

2.2 ACT1A

To obtain better gravity field solutions, a series of calibration processes is applied to ACC1A, providing the calibrated accelerometer data (ACT1A) products (McCullough et al., 2019). Briefly summarized, for GRACE-C, this includes substituting thruster spikes with model values and removing phantom accelerations. The same process is applied to GRACE-D ACC1A until 2018-06-21. Afterwards, following Bandikova et al. (2019), the GRACE-D data is replaced with the transplant data from GRACE-C. ACT1A data are also 10-Hz linear accelerations in AF and OBC time. For more details the reader is referred to Wen et al. (2019) and McCullough et al. (2019).

Figure 2. Schematic view of the axes alignments in the accelerometer reference frame (AF) and the science reference frame (SRF).

Figure 3. ACC compress procedure applied to linear accelerations. This procedure applies time-tag corrections and digital filter on ACT1A accelerometer data to generate ACT1B data.

2.3 ACT1B

During Level-1A to Level-1B data processing, the ACT1A linear accelerations are edited, time tagged and low-pass filtered in order to reduce the high-frequent measurement noise (Wu et al., 2006). Figure 3 describes the Level-1A to Level-1B processing for linear accelerations. The process is discussed in more details in Appendix A. The output of this process is 1-Hz ACT1B product, given in satellite reference frame (SRF) and GPS time.

As the unprocessed Level-1A data products of GRACE-FO are publicly available to all processing centers, an independent Level-1A to Level-1B data processing can be set up. At TUG, we have implemented standard algorithms for data screening, time synchronization and data rate reduction for the raw data, which produce in-house (i.e. independent of the officially released product) ACT1B data, serving as input for the gravity field recovery. To validate the implementation, we compare the TUG ACT1B from GRACE-C with the SDS product. Figure 4 shows time-series and power spectral densities of differences between the two products. The deviations are more than one order of magnitude smaller than the signal noise on each axis, which demonstrates the preciseness of our implementation.

Figure 4. Comparison between the TUG ACT1B and the SDS ACT1B of GRACE-C on July 8, 2018 in time domain (left column) and their differences in frequency domain (right column).

Table 1. Non-gravitational force models due to radiation pressure.

Force Model	References
Solar radiation pressure	Montenbruck and Gill (2000)
Solar flux at 1 AU (1367 $\mathrm{W\,m^{-2}}$)	
Visible and infrared radiation flux	Vielberg and Kusche (2020)
Physical shadow function	Robertson et al. (2015)
Thermal re-radiation	Montenbruck et al. (2014)
Earth radiation pressure	Rodriguez-Solano et al. (2011) and Knocke et al. (1988)
Earth's mean reflectivity and emmisivity*	Wielicki et al. (1996)
Thermal re-radiation	Montenbruck et al. (2014)

*Clouds and the Earth's Radiant Energy System (CERES).

3 Non-gravitational force models

GRACE-FO is operating in a low-Earth orbit (LEO). The non-gravitational accelerations acting upon LEO satellites are mainly due to atmospheric drag, SRP, and ERP. The radiation pressure force models are summarized in Table 1. For the details on the formulae applied for the radiation pressure modeling, the reader is referred to the corresponding references. To model these effects, the satellites' geometry and surface properties are obtained from GRACE-FO macro model (Wen et al., 2019). As the drag force model plays an important role in recovering the GRACE-D missing measurements, the basic equations of respective accelerations are described in the following.

3.1 Atmospheric drag

Aerodynamic force is the force acting on the satellite's surface caused by interchange of momentum with the atmosphere molecules. For LEO satellites, it is the dominant non-gravitational perturbation. The aerodynamic force is modeled as:

$$\boldsymbol{a}_{aero} = -\frac{1}{2}\frac{A_{ref}}{m}\boldsymbol{C}_a \rho {v^2}_{TAS}, \tag{1}$$

depending on the aerodynamic coefficient $\boldsymbol{C}_a$, the atmospheric density ρ, the cross-sectional area A_{ref}, the satellite mass m, and the true airspeed v_{TAS}, i.e. the velocity of the spacecraft relative to the atmosphere. Here, the atmospheric density is obtained from the Jacchia-Bowman 2008 model (JB2008; Bowman et al. (2008)), the cross-sectional area from the macro model and the mass of the satellite are set to their launch mass values, as the MAS1B data product currently do not report the changing satellite mass.

The $\boldsymbol{v}_{TAS}$ is the relative velocity of the satellite with respect to the atmosphere, which is the sum of inertial velocity of the satellite $\dot{\boldsymbol{r}}$, co-rotating atmosphere and atmospheric wind velocity $\boldsymbol{v}_w$:

$$\boldsymbol{v}_{TAS} = \dot{\boldsymbol{r}} - \boldsymbol{\omega}_E \times \boldsymbol{r} + \boldsymbol{v}_w, \tag{2}$$

where $\boldsymbol{r}$ is the satellite position and $\boldsymbol{\omega}_E$ is the angular velocity of the Earth sidereal rotation. The wind velocity is derived from Horizontal Wind Model 2014 (HWM14; Drob et al. (2015)). The component of the aerodynamic force toward normal velocity direction $\hat{\boldsymbol{v}}_{TAS}$ is referred to as drag and the component toward $\frac{\hat{\boldsymbol{v}}_{TAS} \times \hat{\boldsymbol{n}}}{\|\hat{\boldsymbol{v}}_{TAS} \times \hat{\boldsymbol{n}}\|} \times \hat{\boldsymbol{v}}_{TAS}$ as lift, with $\hat{\boldsymbol{n}}$ being the unit normal vector to the satellite plate. Hence, the aerodynamic coefficient can be expressed by:

Figure 5. Comparison between calibrated GRACE-C measurements (black) and simulated data on along-track (blue), cross-track (red), and radial (green) direction on 2019-12-05 (left) and 2019-09-12 (right).

$$\boldsymbol{C}_a = C_D \parallel \hat{\boldsymbol{v}}_{TAS} + C_L \perp \hat{\boldsymbol{v}}_{TAS}. \tag{3}$$

Therein, C_D and C_L are dimensionless drag and lift coefficients, respectively. As drag is the major component of the aerodynamic force acting on satellites, neglecting lift and referring to drag force instead of aerodynamic force is conventional. Consequently, the aerodynamic coefficient can be referred to as drag coefficient, which is set to a constant value of 2.4 for GRACE-FO. Figure 5 shows the summation of non-gravitational models for two days of mission at different β' angles. This comparison reveals that at similar altitude, the maximum acceleration and deviation from model occur when β' is zero and satellite passes through the day-side.

Due to uncertainties in the state and attitude of the satellite, interaction of the satellite's surface and atmosphere molecules affecting the drag coefficient, as well as uncertainties associated with atmospheric density models. It is not possible to model the drag force

Table 2. GRACE-FO science data products required for GRACE-D data recovery.

Data	Description
ACT1A	Calibrated 10-Hz linear acceleration in AF and OBC time
CLK1B	Receiver clock offsets to convert time tags to GPS Time
TIM1B	Time conversion from OBC to receiver time with 8-s sampling
GNV1B	1-Hz satellite's position and velocity, given in Earth-Fixed Frame
SCA1B	1-Hz processed SCA data for rotation from Inertial Frame to SRF
THR1B	Thruster activations given in GPS time

accurately. Therefore, the values used for density and drag coefficient play a significant role in drag model uncertainty (Moe & Moe, 2005; Prieto et al., 2014).

According to Equation 1, drag coefficient and density errors are not completely separable without a good knowledge of at least one of them. Hence, the model exhibits a multiplicative total error from these two sources. However, in case of co-orbiting missions, it is convenient to assume that both satellites experience the same environment, in which the drag model error for each satellite is approximately equivalent. Therefore, by having one actual accelerometer measurements, in this mission GRACE-C, one can estimate the model error, which then can be used to retrieve the missing measurements from the other spacecraft with a malfunctioning accelerometer, i.e GRACE-D.

4 GRACE-D ACC recovery

In the following, the recovery processing for linear accelerations from GRACE-C ACT1A to GRACE-D ACT1B is described. Table 2 summarizes the required data products in this procedure. The input data of the process is the daily 10 Hz GRACE-C ACT1A. In the first step, we apply the standard Level-1A processing, as described in Appendix A, to convert the data to GPS time and SRF frame. Additionally, before applying the low-pass filter, we remove the thruster spikes using THR1B products with a margin of 1 s and fill the gaps with linear interpolation.

4.1 Calibration and Model reduction

The next step is computing the simulated accelerations according to Section 3 for both satellites with 1-Hz sampling. Since orbit data and SCA1B are already created with the same sampling, no interpolation is needed. Using the simulated data, we calibrate the GRACE-C data, obtained from the first step, with daily constant bias on each axis. Lastly, we reduce the simulated data $\boldsymbol{a}_{model}$ from the calibrated GRACE-C data $\boldsymbol{a}_{cal}$, creating the unmodeled acceleration signal $\Delta\boldsymbol{a}$:

$$\Delta\boldsymbol{a} = \boldsymbol{a}_{cal} - \boldsymbol{a}_{model}. \tag{4}$$

4.2 Time correction

In this step, we transfer required GRACE-C Level-1B data, including orbit, SCA1B, and the unmodeled accelerations $\Delta\boldsymbol{a}$ to GRACE-D time frame by applying a transfer time correction. We obtain this correction by using satellites' positions and velocities and solving

Figure 6. Time correction from GRACE-C to GRACE-D on 2018-07-01.

their equations of motions. Figure 6 shows the transfer time correction obtained for 2018-07-01.

4.3 Drag model correction

As mentioned in Section 3, the un-modeled acceleration signal contains an unknown multiplicative error $S_D = \rho \cdot C_D$, i.e. a scale factor, related to atmospheric density and aerodynamic coefficient. Within the recovery process, we estimate this scale factor based on the equation given by:

$$\Delta \boldsymbol{a} = \frac{\partial \Delta \boldsymbol{a}}{\partial S_D} \cdot S_D. \tag{5}$$

To account for temporal variations, the scale value in Eq. 5 is estimated daily, using uniform cubic basis splines (UCBS) (de Boor, 2001). The UCBS is characterized by the degree (d) and the number of knot (k) intervals. Here, we choose a knot interval with 1 min length, which results in $24 \times 60 = 1440$ knots for each daily interval ($k = 1440$). Therefore, the total number of $k + d = 1443$ parameters per interval are needed for the scale estimation. The outputs of this adjustment are: (a) the calculated scale, which will be applied to GRACE-D drag model, and (b) the residual signal, containing errors from other sources as well as the estimation process.

4.4 Attitude correction

The residual signal needs to be transferred to GRACE-D frame by applying attitude correction, as the orientation of each satellite with respect to SRF is different. The K-band ranging (KBR) measurement principle requires precise alignment of each satellite's KBR antenna towards each other, i.e. in the direction of the so-called line of sight (LOS). Since the antenna is mounted at the front panel of each satellite, the leading satellite is turned by 180° around its z-axis. Furthermore, both satellites fly with a pitch offset of approximately 1° with respect to the LOS.

According to Bandikova et al. (2019), for GRACE accelerometer transplant, it was not possible to correct the attitude with the actual attitude variations, due to high-frequency noise on the star camera measurement. Therefore, the attitude correction was approximated by a 180° yaw and an empirical (not physical) 3.2° pitch transform.

In GRACE-FO, the attitude sensors on-board each satellite consist of three star cameras and one angular rate sensing inertial measurement unit (IMU). These attitude data are combined by means of a Kalman filter to obtain an optimal attitude product (SCA1B) (Harvey & Sakumura, 2019). According to (Landerer et al., 2020), this method reduces the noise level by approximately 2 orders of magnitude lower than GRACE. This allows us to directly use the GRACE-FO SCA1B to transfer residual accelerations from GRACE-C to GRACE-D frame.

4.5 Thruster spikes

The final step in the recovery process is to add GRACE-D modeled thruster responses due to attitude thruster firings. This has been done for GRACE-D ACT1A based on regression of the available accelerometer data, as reported by McCullough et al. (2019). To create a Level-1B thruster-only time-series, we compute the difference between two processed GRACE-D ACT1B time-series: one with modeled spikes and the other with removed spikes. For the latter, we remove the thruster events with a margin of 1 s and fill the gaps with linear interpolation during Level-1A processing. The resulting data only includes roll/pitch/yaw thruster firing spikes with 1 s sampling.

5 Results

In the following, we present the comparison of in-house and official ACT1B data sets in time and frequency domain as well as gravity field recovery based on these products.

5.1 GRACE-D accelerations

Figure 7 shows time-series and power spectral densities of differences of the official transplanted data, SDS ACT1B, and the TUG ACT1B. A major difference is visible in radial component, in particular in 1 cycle per revolution (cpr) frequency. As expected, higher frequencies are less affected by the recovery process, as we used the same thruster responses, which are dominant at frequencies over 3 mHz. Figure 8 reveals that the magnitude of the differences between the SDS and TUG data is dependant on orbit configuration with respect to Sun, i.e. β' angle. Here, for all components, major differences exist at 1-3 cpr frequencies. For further details, the differences are plotted as a function of argument of latitude and time in Figure 9. It is visible that the recovery process mainly affects radial and along-track components, when satellites are directly illuminated by the Sun ($\beta' \sim 0°$).

5.2 Drag model scale

As depicted in Section 4, we estimate drag model scale factors during the GRACE-D ACC recovery process. Figure 10 illustrates the time series of the estimated scale. The estimates show scattered variations comparable with β' angle cycle. This behavior reflects the higher uncertainties in atmosphere density during periods with direct sunlight, i.e. with β' angle ranging from $-20°$ to $30°$. To some extent the variations of the estimated values also depends on the temperature fluctuations in these periods, which affects the gas molecular behavior and therefore, the drag coefficient.

Additionally, the high-frequency perturbations of the atmospheric density during geomagnetic storms are also expected to be absorbed by the scale factors. However, our observations are mainly collected during solar minimum (2018-2020) and, therefore, sparse solar events are visible in the data. During this period, the severest geomagnetic storm

Figure 7. Comparison of the time-series (left) and power spectral densities of differences (right) of the SDS ACT1B and the TUG ACT1B on 2020-05-13, with indirect sunlight condition ($\beta' = 71.8°$).

Figure 8. Comparison of the time-series (left) and power spectral densities of differences (right) of the SDS ACT1B and the TUG ACT1B on 2020-07-31, with direct sunlight condition ($\beta' = -0.4°$).

Figure 9. Differences between the SDS transplanted data and the TUG data from July 2018 to August 2020, plotted with respect to GRACE-C argument of latitude. Major differences are visible in radial direction under direct Sun exposure.

Figure 10. Temporal variations of (a) the estimated drag scale, (b) the corresponding β' angle variations, and (c) thermosphere temperature derived from JB2008 model, from May 2018 to August 2020.

Figure 11. Temporal variation of the estimated drag scale, compared to the SYM-H index during minor geomagnetic events in (a) May and (b) August 2019.

happened on 26 August 2018, whose impact on GRACE-C accelerometer measurements has been studied by Krauss et al. (2020). Due to the gaps in GRACE-D data, this period is not included in the scale time series. Nevertheless, few minor geomagnetic storms have triggered atmospheric disturbances during 2019 and 2020 and subsequently affected the scale factors.

Among a variety of indices, which characterize the geomagnetic activities, it has been shown that the SYM-H index (Iyemori et al., 2010) has one of the highest correlation with the neutral atmospheric density, with nearly zero time delay at low earth orbiters (Krauss et al., 2015). SYM-H index describes the geomagnetic disturbances at mid-latitudes with a temporal resolution of 1 minute. Figure 11 shows the time series of the estimated scale, compared to the variations of this index. For two selected events, a clear correlation exists between peaks in SYM-H and scale factor time series.

It is worth mentioning that in addition to the described effects, the estimates probably absorb other effects, which are not adequately modeled (e.g. variations in radiation pressure models).

5.3 Gravity field

This section compares the monthly gravity field solutions based on the recovered GRACE-D accelerometer data and ITSG-Grace2018 scheme (Kvas, Behzadpour, et al., 2019). We recovered monthly solutions from July 2018 to August 2020 using (a) SDS ACT1B in preliminary results, denoted as ITSG-Grace2018p, and (b) TUG ACT1B in

Figure 12. Degree amplitudes of coefficient differences of the CSR RL06 solution (green), the ITSG-Grace2018 (prelim.) solution (blue), and the ITSG-Grace2018 solution (red) for July 2020 w.r.t the GOCO06s model.

final GRACE-FO operational solutions, referred to as ITSG-Grace2018. The ITSG-Grace2018 solutions are publicly available and can be downloaded from ICGEM site (http://icgem.gfz-potsdam.de/ or ifg.tugraz.at/ITSG-Grace2018).

Figure 12 shows the degree variances for July 2020 ($\beta' = -0.4°$) with respect to the static gravity field GOCO06s (Kvas, Mayer-Gürr, et al., 2019). Compared to the preliminary solution, ITSG-Grace2018 with in-house computed ACT1B performs better in terms of noise over all spherical harmonic degrees, with the largest differences in degree 2 and 3.

Figure 13 shows the power spectral densities of the post-fit range rate residuals from both solutions (ITSG-Grace2018p and ITSG-Grace2018). The post-fit residuals are the differences between adjusted and original range rate observations. The residuals indicate the total error sources, which are present within the gravity recovery process, as they are propagated errors of all involved instruments and modeling errors. Here, strong 2 cpr and 3 cpr signals, existing in the preliminary scenario, are mitigated using the GRACE-D TUG ACT1B. This clearly demonstrates the overall improvement of gravity field solutions and better estimation of low degree coefficients, particularly C_{20} and C_{30}.

For more details, we compare the monthly estimates of C_{20} derived from GRACE-FO and SLR-derived values, provided in the TN-14, over the entire available period. Figure 14a shows that the bias in the estimates from ITSG-Grace2018 solutions has reduced with respect to the TN-14 values. However, similar to GRACE, the C_{20} coefficients still exhibit a strong 161-day periodic signal and should be replaced by C_{20} estimates from SLR data.

Figure 13. PSD of the post-fit range-rate residuals from the ITSG-Grace2018 (prelim.) solution (blue) and the ITSG-Grace2018 solution (red) for July 2020.

Figure 14. Comparison of (a) C_{20} and (b) C_{30} estimates from GRACE-FO monthly gravity field solutions (CSR RL06 (green), ITSG-Grace2018p (blue), ITSG-Grace2018 (red)) and from recommended SLR derived values in Technical Note-14 (black)).

Additionally, Figure 14b demonstrates the C_{30} time-series derived from GRACE-FO and SLR. The ITSG-Grace2018 estimates for the C_{30} coefficients show a higher correlation with the SLR solution. This supports the hypothesis that by mitigating 2 cpr and 3 cpr signals in transplanted data, resulting from alternative GRACE-D ACT recovery, the estimates of the C_{30} coefficients are significantly improved. The improvement is mainly visible for the months with $\beta' \sim 0°$.

6 Conclusions

The results presented in this paper show the advantages of incorporating non-gravitational force models and applying drag model corrections within GRACE-D ACC recovery. The alternative ACT product contributes to an improved estimation of higher degrees of the recovered monthly gravity field solutions, as well as low zonal degrees 2 and 3. The estimates of the C_{30} coefficients represents a significant improvement with respect to SLR-derived values, with which the GRACE-FO values are recommended to be substituted.

Additionally, we were able to prove that the non-gravitational forces, in particular the corrected drag model, recover part of the acceleration signal that is missing in the direct transplant approach in radial and along-track directions. The magnitude of this missing signal is β' angle dependant and reaches its maximum during direct Sun exposure. Within the periods of passing the Earth's shadow, the modeled signal is approximately zero.

Furthermore, we show that the drag model scale correction mainly reflects the physical characterizations of changing thermospheric density. This includes long-term variations during periods with direct sunlight, as well as short-term fluctuations due to geomagnetic storms.

However, there are several issues, which have a potential for further improvements: In order to avoid the effects from outliers in GRACE-C measurements, the parameterization of the drag scale reflects smoothed variations longer than 1 minute. This setup may result in losing high-frequency details in the satellites' changing environment. Moreover, thruster spikes, which also contributes to the high-frequency spectrum of the measurements, are currently modeled with simple impulse functions with constant magnitudes based on statistical estimation. As proved in GRACE mission (Bandikova et al., 2019), incorporating more realistic thruster responses in transplant data considerably reduces noise in degrees over 15, i.e. the first orbital resonance.

In summary, this work contributes to an improvement of the GRACE-FO derived gravity field solutions by investigating the role of the missing GRACE-D accelerometer data. The efforts in constructing the constituents of the missing measurements not only increase the gravity field quality, but also improve our knowledge about satellites' interaction with their environment.

Appendix A ACT Level1-A processing

In the following, the accelerometer Level-1A (ACT1A) to Level-1B (ACT1B) processing for linear accelerations is described, based on Wu et al. (2006). The ACC processing includes the following steps:

1. Level-1A accelerometer (ACC1A), clock (CLK1B), and time (TIM1B) data products are read and converted.
2. Invalid data from (1), flagged with "no pulse sync" or "invalid timetag", are removed.
3. The accelerometer time-tags are converted from OBC time to receiver time. In order to convert the OBC time to receiver time, a correction has to be applied from the TIM1B data product.

4. Linear accelerometer data is re-sampled to integer multiples of 0.1 s (10 Hz) using linear interpolation.
5. The data gaps are filled using cubic interpolation with up to 200 data points on each side of the gap. If a data gap is larger than 100 s, no filling is made.
6. The accelerometer time tags are converted from GPS receiver time to GPS time. Computation of the time-tag corrections is by linearly interpolating the clock corrections from the input CLK1B data product. If there is no valid clock correction data for a time span, the clock corrections are extrapolated using the valid clock corrections outside this time span. This guarantees continuity of the ACC data. Additionally, the Butterworth filter delay of nominally 0.14 s has to be considered.
7. Linear accelerations are re-sampled to integer multiples of 0.1 s using a Lagrange quadratic interpolation over the nearest 3 data points.
8. The ACC data is compressed with a digital CRN filter of 7th order self-convolution with 35 mHz bandwidth over a 140.7 s data span.
9. The sampling of the filtered linear ACC data is reduced from 0.1 s to 1 s by removing the additional data epochs from the filtered data.
10. The ACC data is transformed from the AF to the SRF and writing the output accelerometer ACC1B data files.

Acknowledgments

We would like to thank the German Space Operations Center (GSOC) of the German Aerospace Center (DLR) for providing continuously and nearly 100% of the raw telemetry data of the twin GRACE-FO satellites. The GRACE-FO Level-1 and Level-2 data used in this study can be obtained from the NASA's Physical Oceanography Distributed Active Archive Center (`https://podaac.jpl.nasa.gov/GRACE-FO`) and the GFZ's Information System and Data Center (`ftp://isdcftp.gfz-potsdam.de/grace-fo/`).

Furthermore, we are grateful and acknowledge the JB2008 data courtesy of Space Environment Technologies for providing us the forecasting values for the JB2008 model.

This work is funded by the Austrian Research Promotion Agency (FFG) in the frame of the Austrian Space Applications Programme Phase 15 (Project 873668), and by The Global Gravity-based Groundwater Product (G3P) project in the framework of the European Union's Horizon 2020 research and innovative programme under grant agreement No.870353.

References

Bandikova, T., McCullough, C., Kruizinga, G. L., Save, H., & Christophe, B. (2019). GRACE accelerometer data transplant. *Advances in Space Research*, *64*(3), 623 - 644. doi: 10.1016/j.asr.2019.05.021

Bowman, B., Tobiska, W. K., Marcos, F., Huang, C., Lin, C., & Burke, W. (2008). A new empirical thermospheric density model JB2008 using new solar and geomagnetic indices. In *AIAA/AAS astrodynamics specialist conference and exhibit.* American Institute of Aeronautics and Astronautics. doi: 10.2514/6.2008-6438

Christophe, B., Boulanger, D., Foulon, B., Huynh, P.-A., Lebat, V., Liorzou, F., & Perrot, E. (2015). A new generation of ultra-sensitive electrostatic accelerometers for grace follow-on and towards the next generation gravity missions. *Acta Astronautica*, *117*, 1 - 7. doi: 10.1016/j.actaastro.2015.06.021

de Boor, C. (2001). *A practical guide to splines*. New York: Springer Verlag.

Drewes, H., Kuglitsch, F., Adám, J., & Rózsa, S. (2016). The geodesist's handbook 2016. *Journal of Geodesy*, *90*(10), 907–1205. doi: 10.1007/s00190-016-0948-z

Drob, D. P., Emmert, J. T., Meriwether, J. W., Makela, J. J., Doornbos, E., Conde, M., ... Klenzing, J. H. (2015). An update to the horizontal wind model (HWM): The

quiet time thermosphere. *Earth and Space Science*, *2*(7), 301–319. doi: 10.1002/2014ea000089

Harvey, N., & Sakumura, C. (2019). Results from a GRACE/GRACE-FO attitude reconstruction kalman filter. *Journal of Geodesy*, *93*(10), 1881–1896. doi: 10.1007/s00190-019-01289-z

Iyemori, T., Takeda, M., Nose, M., Odagi, Y., & Toh, H. (2010). *Mid-latitude Geomagnetic Indices ASY and SYM for 2009* (Tech. Rep.). Internal Report of Data Analysis Center for Geomagnetism and Space Magnetism, Kyoto University, Japan. Retrieved from `http://wdc.kugi.kyoto-u.ac.jp/aeasy/asy.pdf`

Knocke, P., Ries, J., & Tapley, B. (1988). Earth radiation pressure effects on satellites. In *Astrodynamics conference.* American Institute of Aeronautics and Astronautics. doi: 10.2514/6.1988-4292

Krauss, S., Behzadpour, S., Temmer, M., & Lhotka, C. (2020). Exploring thermospheric variations triggered by severe geomagnetic storm on 26 august 2018 using GRACE follow-on data. *Journal of Geophysical Research: Space Physics*, *125*(5). doi: 10.1029/2019ja027731

Krauss, S., Temmer, M., Veronig, A., Baur, O., & Lammer, H. (2015). Thermospheric and geomagnetic responses to interplanetary coronal mass ejections observed by ACE and GRACE: Statistical results. *Journal of Geophysical Research A: Space Physics*, *120*(10). doi: 10.1002/2015JA021702

Kvas, A., Behzadpour, S., Ellmer, M., Klinger, B., Strasser, S., Zehentner, N., & Mayer-Gürr, T. (2019). ITSG-Grace2018: Overview and evaluation of a new GRACE-only gravity field time series. *Journal of Geophysical Research: Solid Earth*, *124*(8), 9332–9344. doi: 10.1029/2019jb017415

Kvas, A., Mayer-Gürr, T., Krauss, S., Brockmann, J. M., Schubert, T., Schuh, W.-D., ... Meyer, U. (2019). *The satellite-only gravity field model GOCO06s.* GFZ Data Services. Retrieved from `https://dataservices.gfz-potsdam.de/icgem/showshort.php?id=escidoc:4081892` doi: 10.5880/ICGEM.2019.002

Landerer, F. W., Flechtner, F. M., Save, H., Webb, F. H., Bandikova, T., Bertiger, W. I., ... Yuan, D.-N. (2020). Extending the global mass change data record: GRACE follow-on instrument and science data performance. *Geophysical Research Letters*, *47*(12). doi: 10.1029/2020gl088306

Loomis, B. D., Rachlin, K. E., Wiese, D. N., Landerer, F. W., & Luthcke, S. B. (2020). Replacing GRACE/GRACE-FO with satellite laser ranging: Impacts on antarctic ice sheet mass change. *Geophysical Research Letters*, *47*(3). doi: 10.1029/2019gl085488

McCullough, C., Bettadpur, S., & McDonald, K. (2015). Accuracy of numerical algorithms for satellite orbit propagation and gravity field determination. *Journal of Spacecraft and Rockets*, *52*(3), 766–775. doi: 10.2514/1.a33008

McCullough, C., Harvey, N., Save, H., & Bandikova, T. (2019). *Description of Calibrated GRACE-FO Accelerometer Data Products (ACT), Level-1 Product Version 04* (Tech. Rep. No. JPL D-103863). Jet Propulsion Laboratory, Pasadena, California. Retrieved from `https://podaac-tools.jpl.nasa.gov/drive/files/allData/grace/docs/ATBD_L1B_v1.2.pdf`

Meyer, U., Jäggi, A., & Beutler, G. (2011). The impact of attitude control on GRACE accelerometry and orbits. In *Geodesy for Planet Earth* (pp. 139–146). Springer Berlin Heidelberg. doi: 10.1007/978-3-642-20338-1_17

Moe, K., & Moe, M. M. (2005). Gas–surface interactions and satellite drag coefficients. *Planetary and Space Science*, *53*(8), 793–801. doi: 10.1016/j.pss.2005.03.005

Montenbruck, O., & Gill, E. (2000). *Satellite orbits.* Springer Berlin Heidelberg. doi: 10.1007/978-3-642-58351-3

Montenbruck, O., Steigenberger, P., & Hugentobler, U. (2014). Enhanced solar radiation pressure modeling for Galileo satellites. *Journal of Geodesy*, *89*(3), 283–297. doi: 10.1007/s00190-014-0774-0

Prieto, D. M., Graziano, B. P., & Roberts, P. C. (2014). Spacecraft drag modelling. *Progress in Aerospace Sciences*, *64*, 56–65. doi: 10.1016/j.paerosci.2013.09.001

Robertson, R., Flury, J., Bandikova, T., & Schilling, M. (2015). Highly physical penumbra solar radiation pressure modeling with atmospheric effects. *Celestial Mechanics and Dynamical Astronomy*, *123*(2), 169–202. doi: 10.1007/s10569-015-9637-0

Rodriguez-Solano, C. J., Hugentobler, U., & Steigenberger, P. (2011). Impact of albedo radiation on GPS satellites. In *Geodesy for planet earth* (pp. 113–119). Springer Berlin Heidelberg. doi: 10.1007/978-3-642-20338-1_14

Save, H. V., Bettadpur, S. V., & Tapley, B. D. (2006). Single Accelerometer Gravity Solutions for GRACE. AGU Fall Meeting, abstract G13A-0026.

Tapley, B. D., Bettadpur, S., Watkins, M., & Reigber, C. (2004). The gravity recovery and climate experiment: Mission overview and early results. *Geophysical Research Letters*, *31*(9). doi: 10.1029/2004gl019920

Vielberg, K., & Kusche, J. (2020). Extended forward and inverse modeling of radiation pressure accelerations for LEO satellites. *Journal of Geodesy*, *94*(4). doi: 10.1007/s00190-020-01368-6

Wen, H. Y., Kruizinga, G., Paik, M., Landerer, F., Bertiger, W., Sakumura, C., ... McCullough, C. (2019). *Gravity Recovery and Climate Experiment Follow-On (GRACE-FO) Level-1 Data Product User Handbook* (Tech. Rep. No. JPL D-56935 (URS270772)). Jet Propulsion Laboratory, Pasadena, California. Retrieved from `https://podaac-tools.jpl.nasa.gov/drive/files/allData/gracefo/docs/GRACE-FO_L1_Handbook.pdf`

Wielicki, B. A., Barkstrom, B. R., Harrison, E. F., Lee, R. B., Smith, G. L., & Cooper, J. E. (1996). Clouds and the earths radiant energy system (CERES): An earth observing system experiment. *Bulletin of the American Meteorological Society*, *77*(5), 853–868. doi: 10.1175/1520-0477(1996)077⟨0853:catere⟩2.0.co;2

Wu, S.-C., Kruizinga, G., & Bertiger, W. (2006). *Algorithm Theoretical Basis Document for GRACE Level-1B Data Processing V1.2* (Tech. Rep. No. GRACE 327-741). Jet Propulsion Laboratory, Pasadena, California. Retrieved from `https://podaac-tools.jpl.nasa.gov/drive/files/allData/grace/docs/ATBD_L1B_v1.2.pdf`

Figure 01.

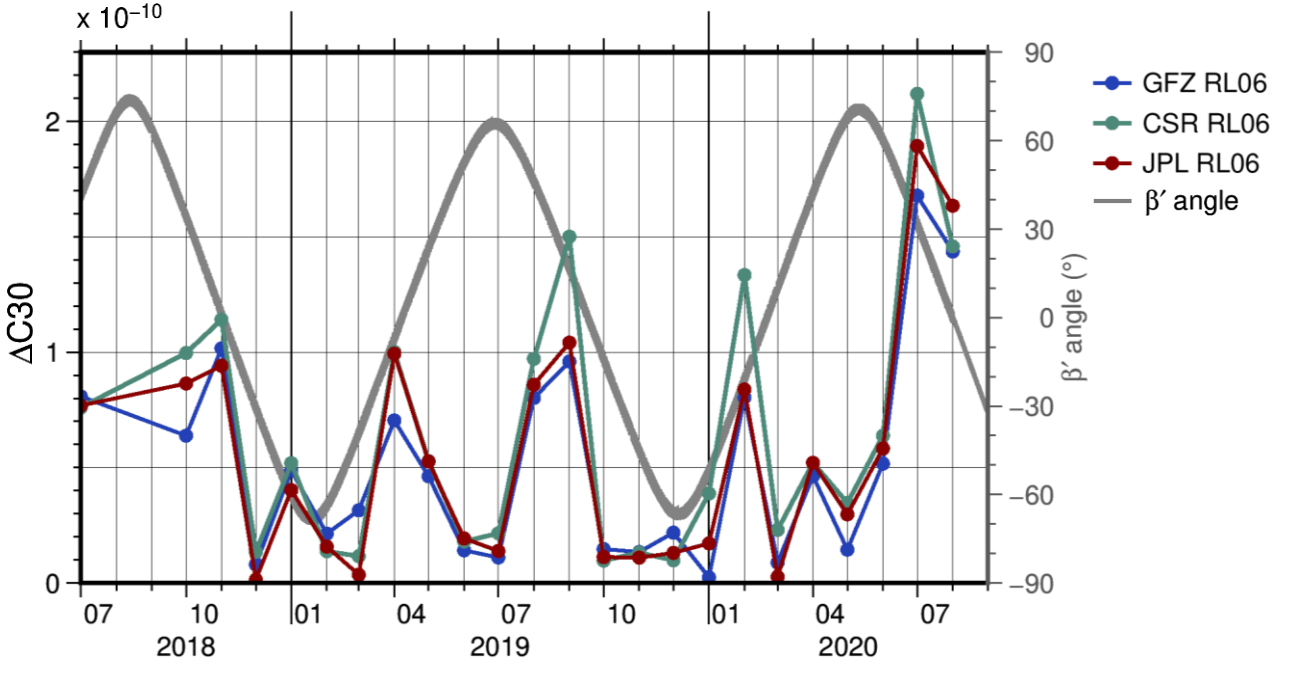
x 10−10
ΔC30
2
1
0
90
60
30
0
−30
−60
−90
β′ angle (°)
GFZ RL06
CSR RL06
JPL RL06
β′ angle
07
10
01
04
07
10
01
04
07
2018
2019
2020

Figure 02.

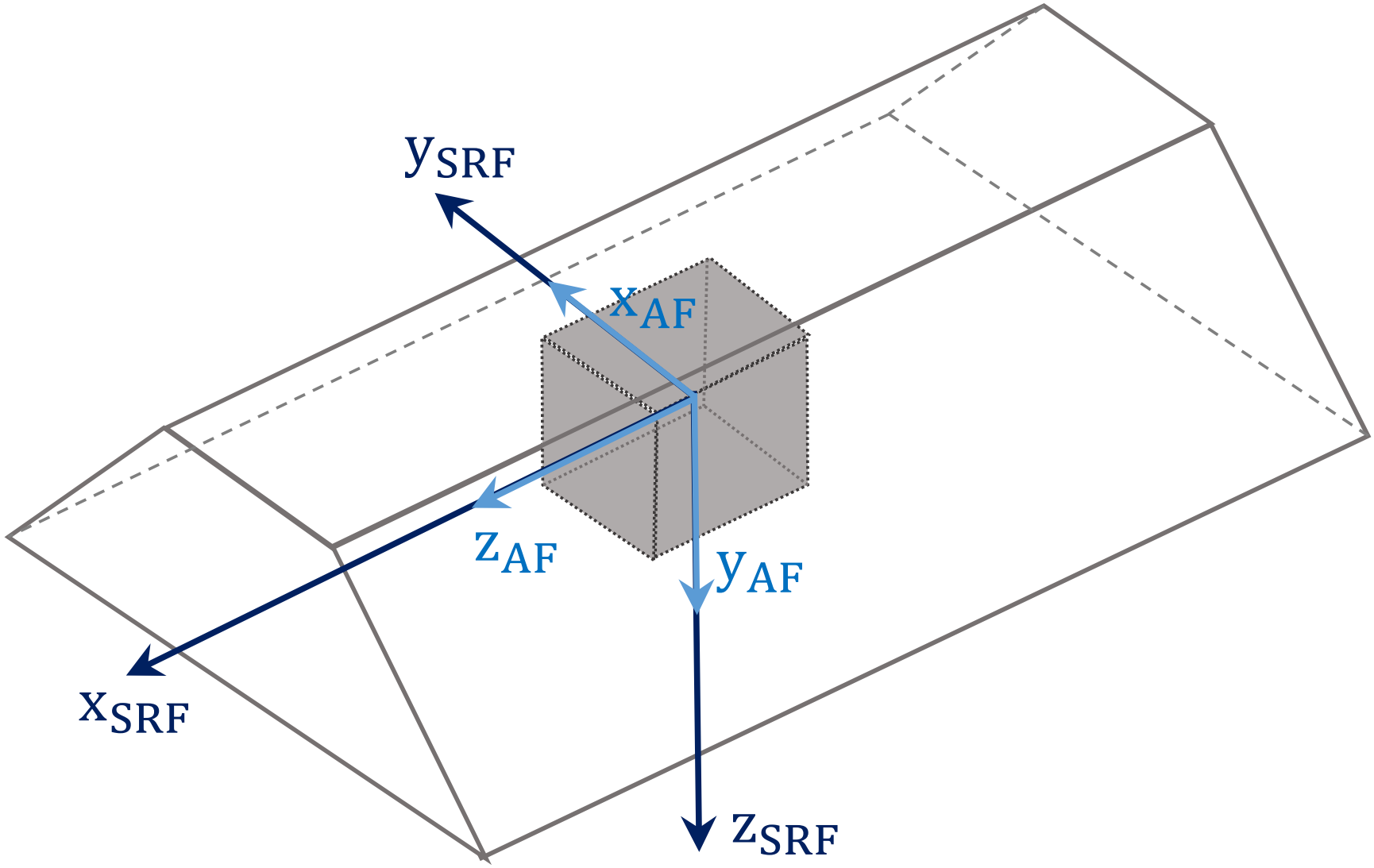
y_{SRF}
x_{AF}
z_{AF}
y_{AF}
x_{SRF}
z_{SRF}

Figure 03.

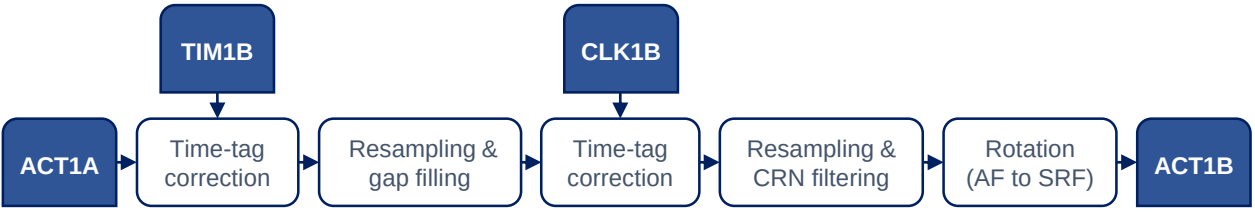
TIM1B
CLK1B
ACT1A
Time-tag correction
Resampling & gap filling
Time-tag correction
Resampling & CRN filtering
Rotation (AF to SRF)
ACT1B

Figure 04.

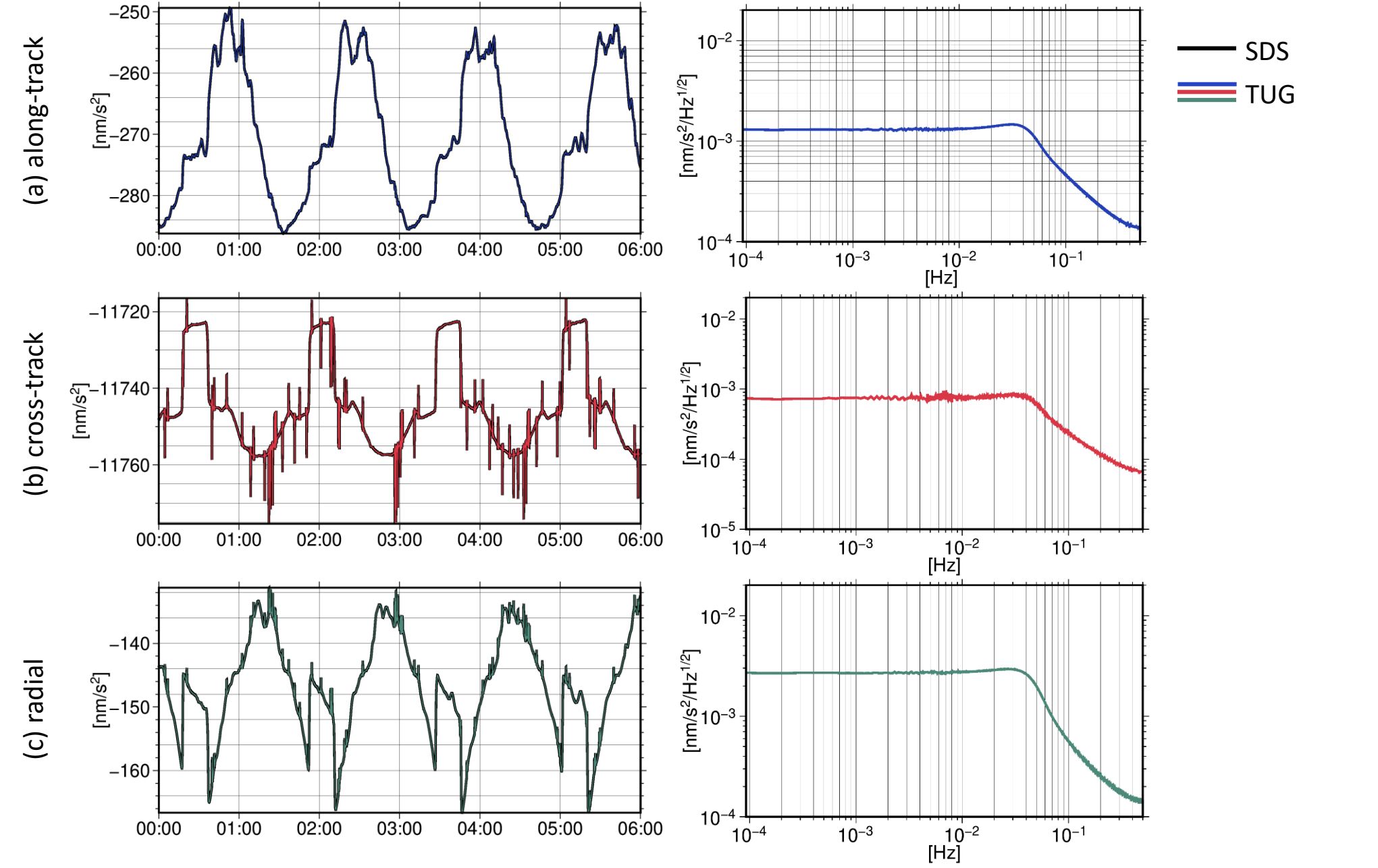
(a) along-track
(b) cross-track
(c) radial
[nm/s²]
−250
−260
−270
−280
−11720
−11740
−11760
−140
−150
−160
00:00
01:00
02:00
03:00
04:00
05:00
06:00
[nm/s²/Hz^1/2]
10⁻²
10⁻³
10⁻⁴
10⁻⁵
[Hz]
SDS
TUG

Figure 05.

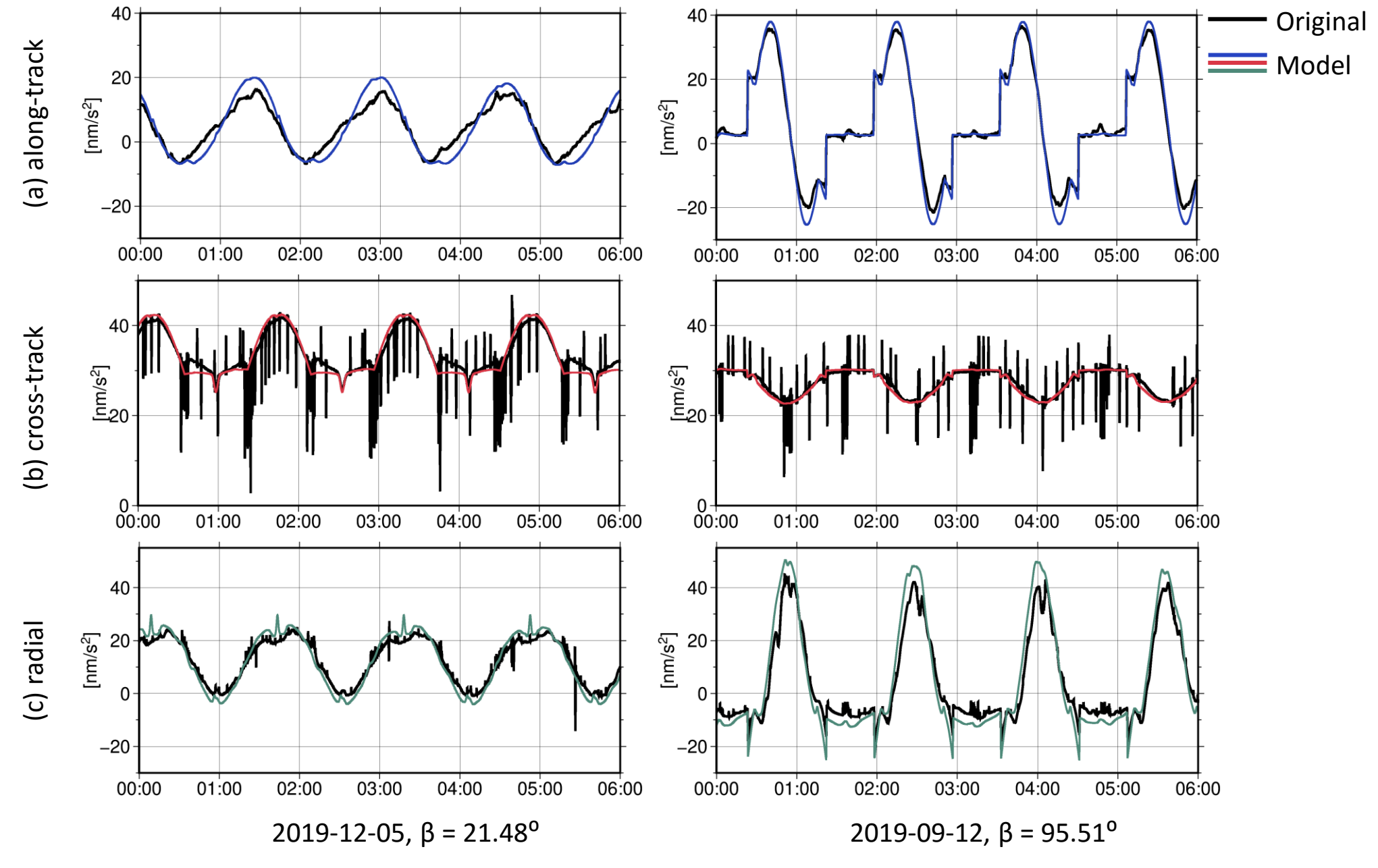
(a) along-track
(b) cross-track
(c) radial
[nm/s²]
40
20
0
−20
00:00
01:00
02:00
03:00
04:00
05:00
06:00
Original
Model
2019-12-05, β = 21.48°
2019-09-12, β = 95.51°

Figure 06.

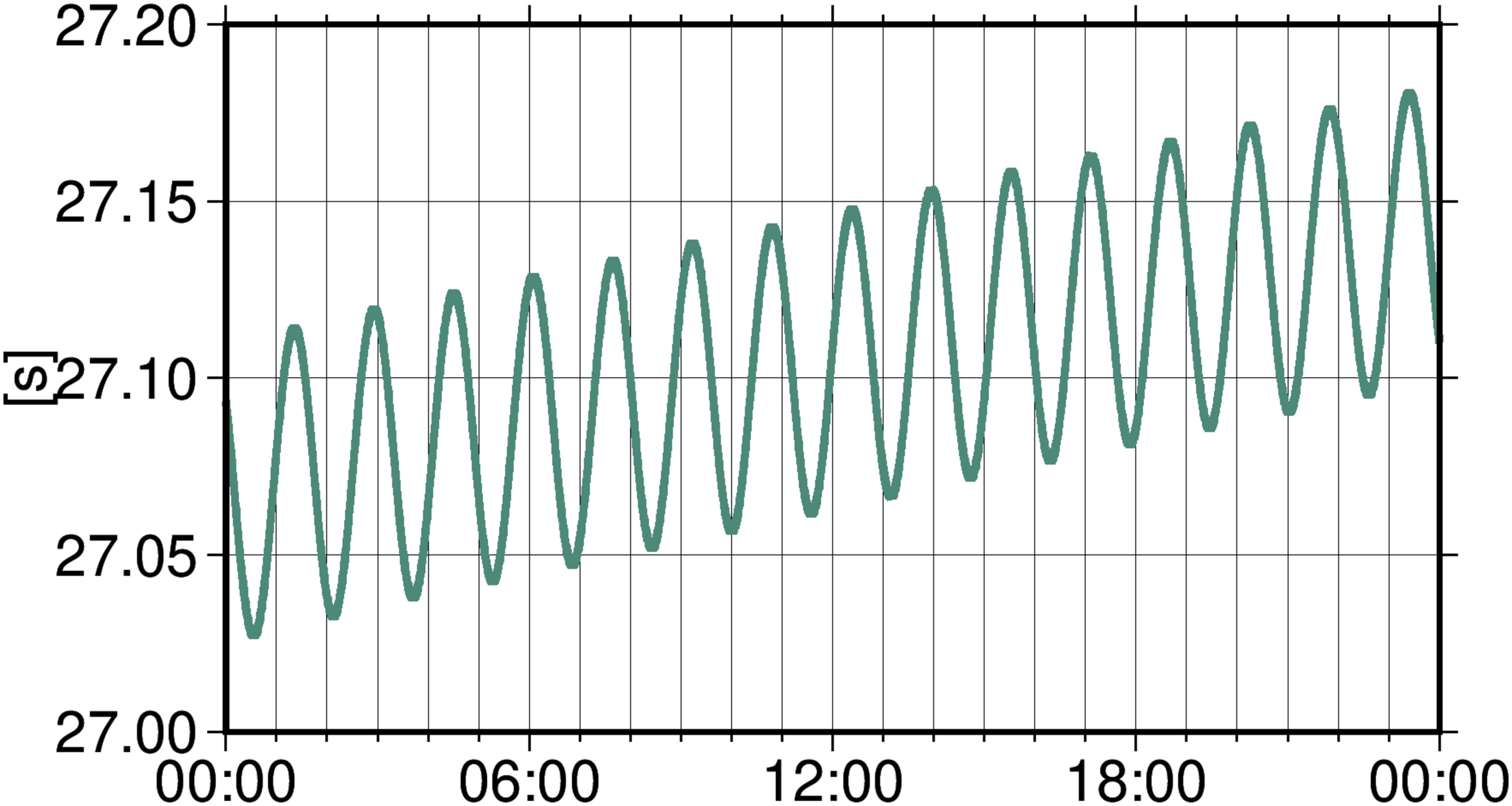
27.20
27.15
27.10
27.05
27.00
[s]
00:00
06:00
12:00
18:00
00:00

Figure 07.

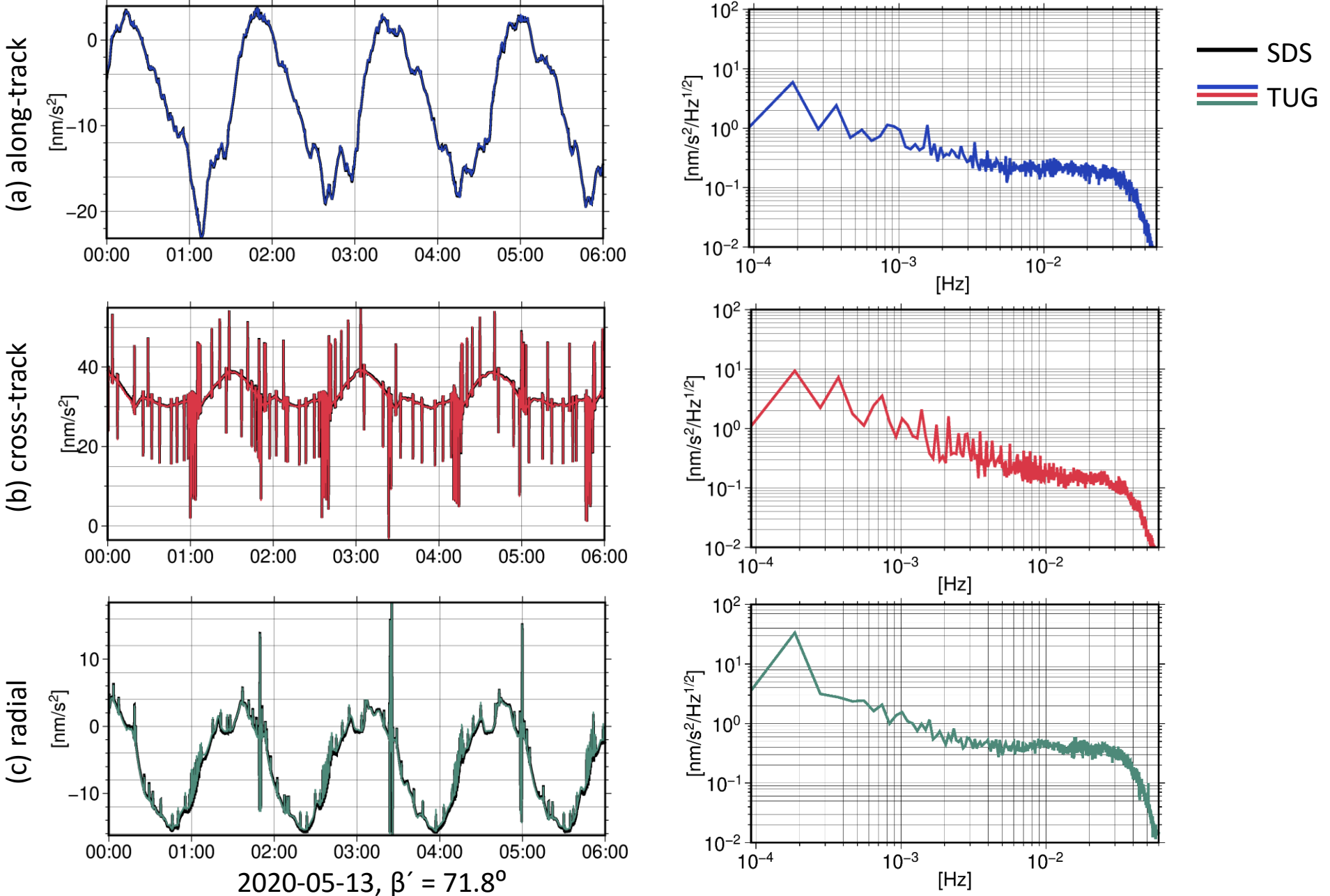
(a) along-track
(b) cross-track
(c) radial
[nm/s²]
00:00
01:00
02:00
03:00
04:00
05:00
06:00
[nm/s²/Hz^1/2]
[Hz]
SDS
TUG
2020-05-13, β´ = 71.8°

Figure 08.

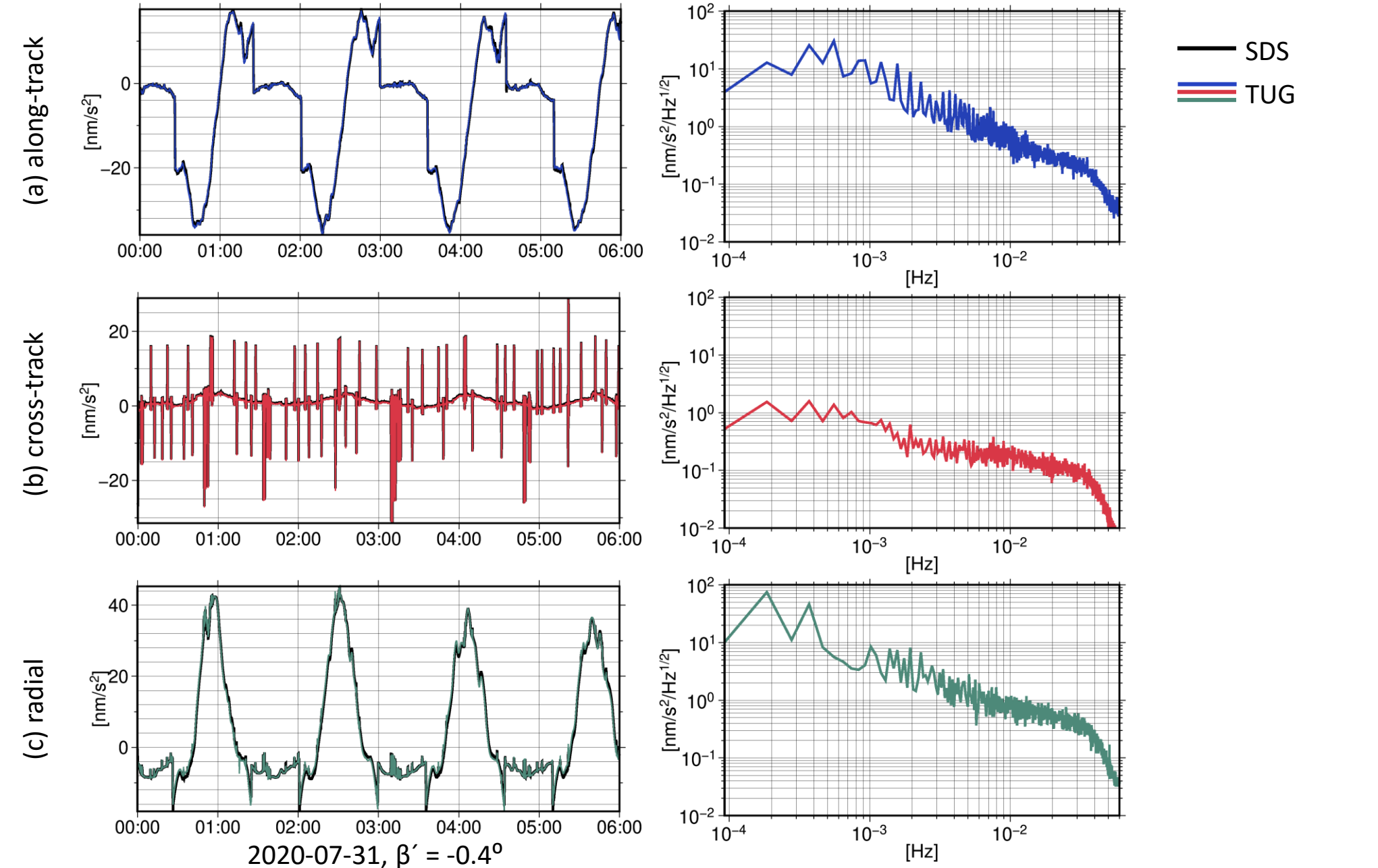
(a) along-track
(b) cross-track
(c) radial
[nm/s²]
00:00
01:00
02:00
03:00
04:00
05:00
06:00
[nm/s²/Hz^1/2]
[Hz]
SDS
TUG
2020-07-31, β´ = -0.4°

Figure 09.

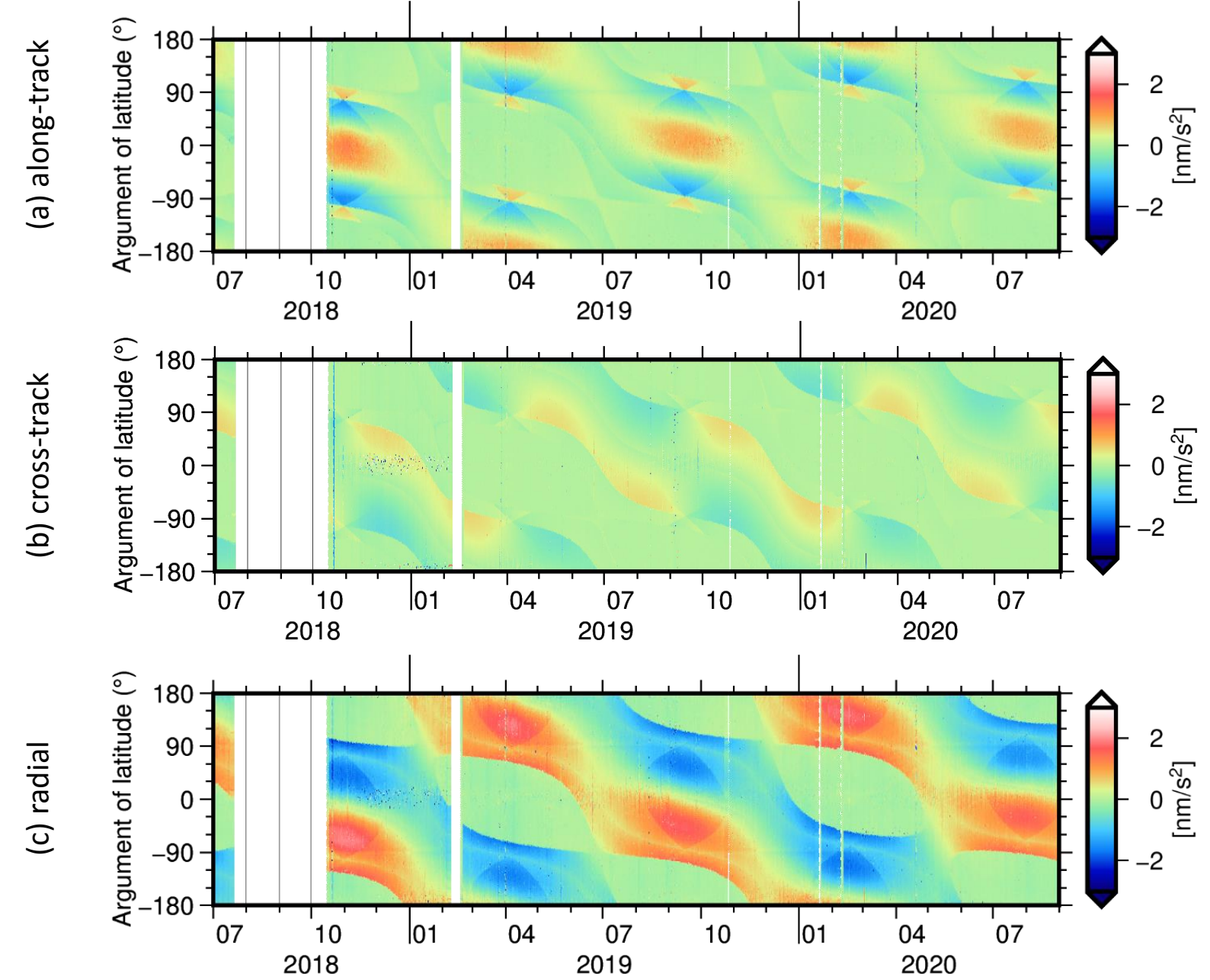
(a) along-track
(b) cross-track
(c) radial
Argument of latitude (°)
180
90
0
−90
−180
07
10
01
04
07
10
01
04
07
2018
2019
2020
2
0
−2
[nm/s²]

Figure 10.

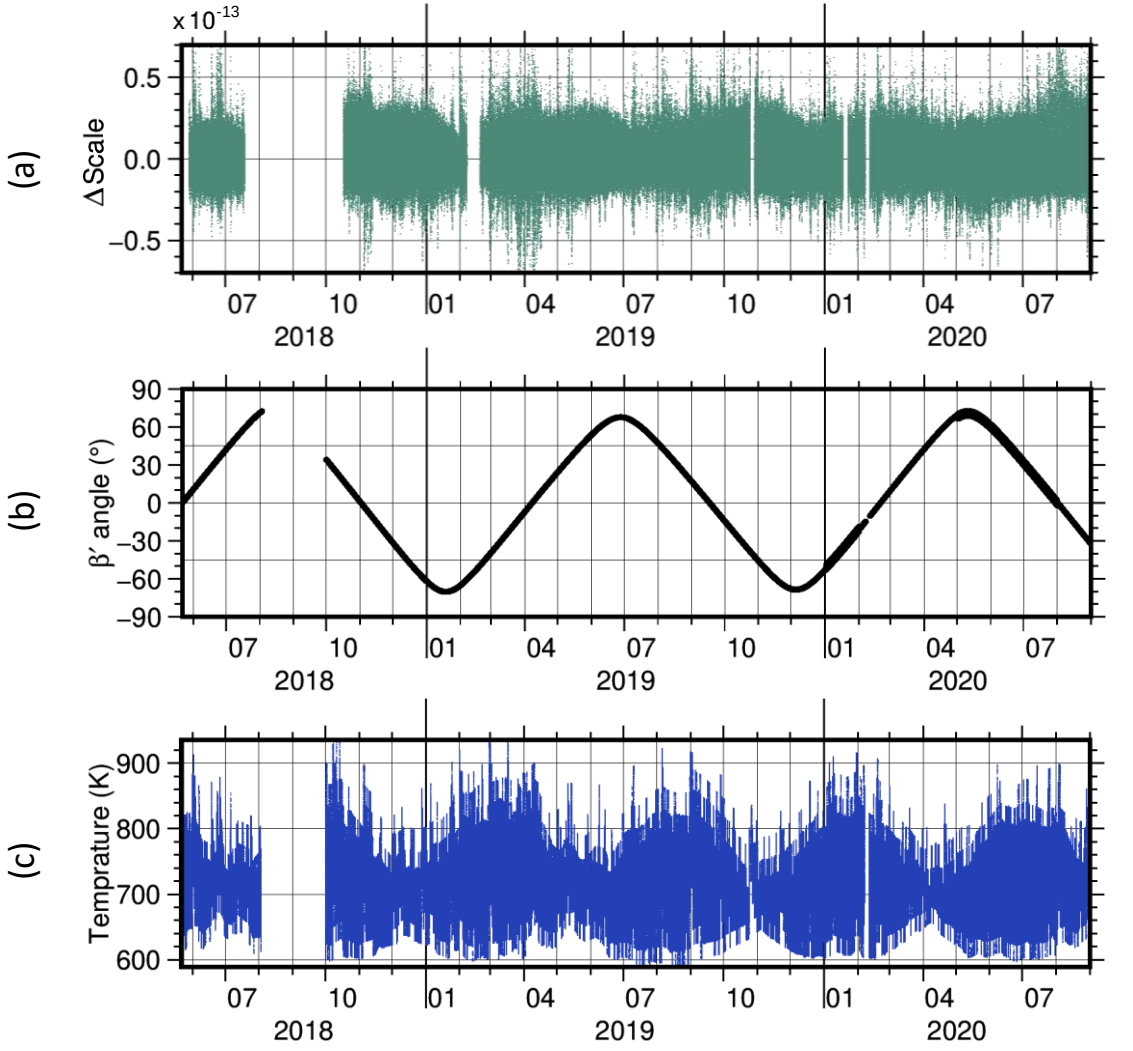
(a)
x 10^-13
ΔScale
0.5
0.0
−0.5
07
10
01
04
07
10
01
04
07
2018
2019
2020
(b)
β′ angle (°)
90
60
30
0
−30
−60
−90
07
10
01
04
07
10
01
04
07
2018
2019
2020
(c)
Temprature (K)
900
800
700
600
07
10
01
04
07
10
01
04
07
2018
2019
2020

Figure 11.

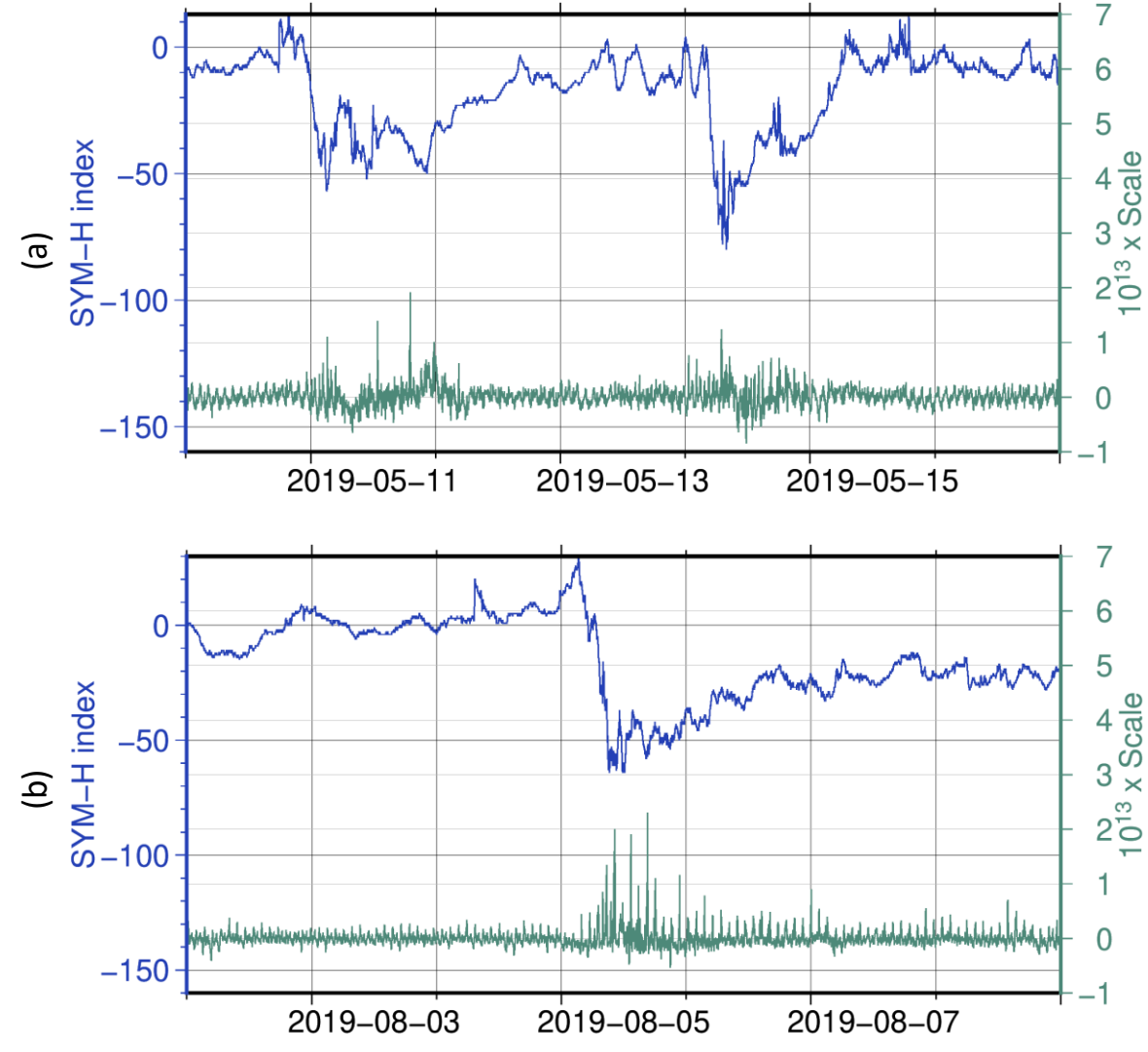
(a)
SYM–H index
0
−50
−100
−150
7
6
5
4
3
2
1
0
−1
10^{13} x Scale
2019–05–11
2019–05–13
2019–05–15
(b)
SYM–H index
0
−50
−100
−150
7
6
5
4
3
2
1
0
−1
10^{13} x Scale
2019–08–03
2019–08–05
2019–08–07

Figure 12.

2020–07

10^{-2}

10^{-3}

10^{-4}

10^{-5}

Geoid height [m]

0

30

60

90

Degree

CSR RL06

ITSG–Grace2018p

ITSG–Grace2018

Figure 13.

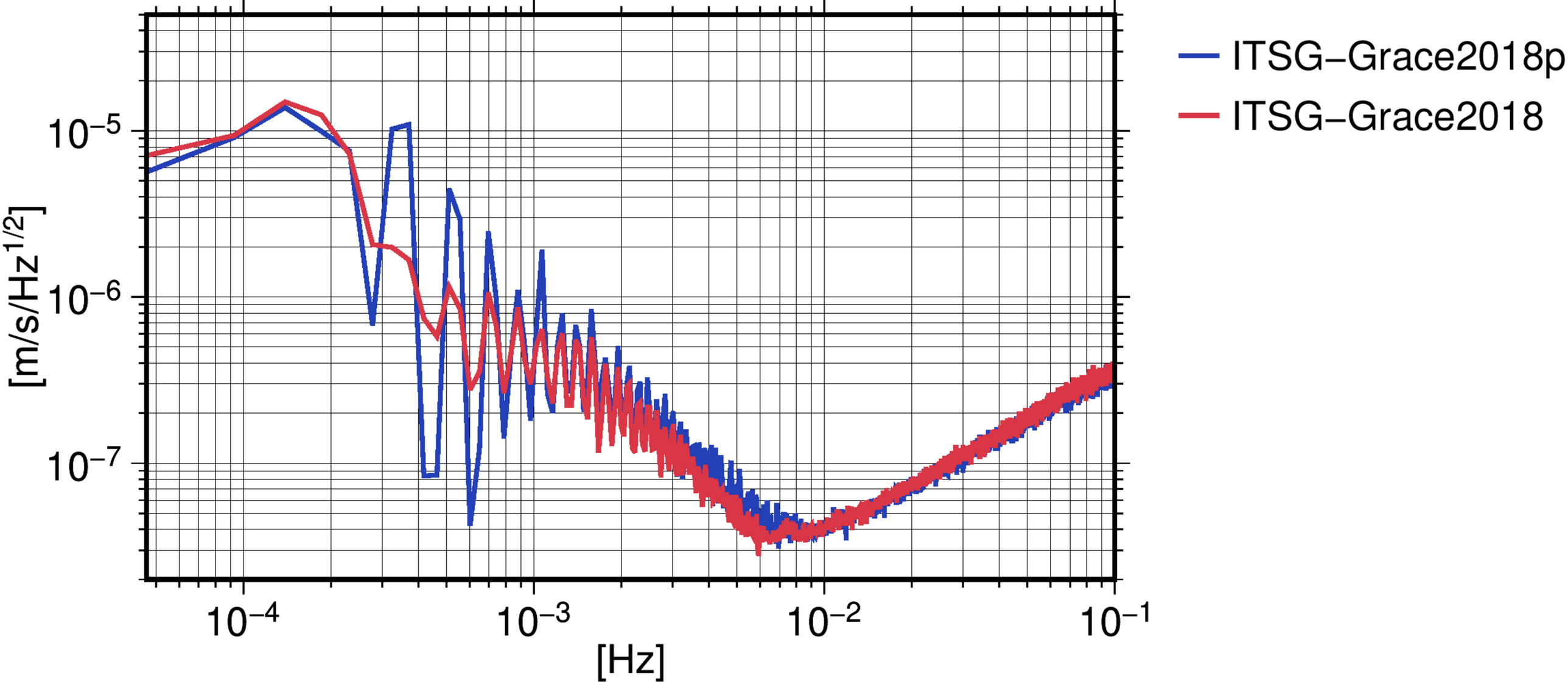
ITSG–Grace2018p
ITSG–Grace2018
10^{-5}
10^{-6}
10^{-7}
[m/s/Hz$^{1/2}$]
10^{-4}
10^{-3}
10^{-2}
10^{-1}
[Hz]

Figure 14.

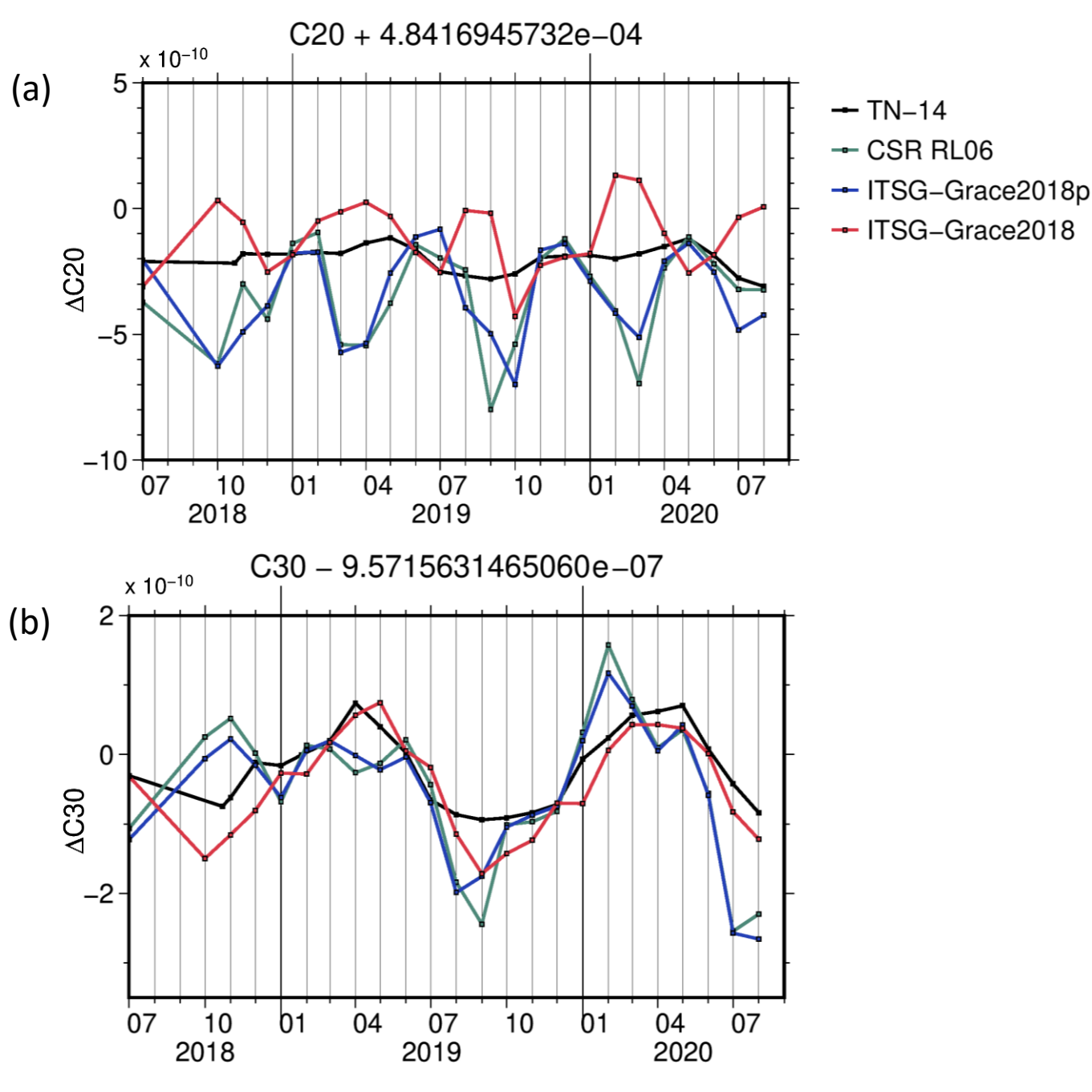
(a)
C20 + 4.8416945732e−04
x 10−10
5
0
−5
−10
ΔC20
07
10
01
04
07
10
01
04
07
2018
2019
2020
TN−14
CSR RL06
ITSG−Grace2018p
ITSG−Grace2018
(b)
C30 − 9.5715631465060e−07
x 10−10
2
0
−2
ΔC30
07
10
01
04
07
10
01
04
07
2018
2019
2020